Methyl-group dynamics from tunneling to hopping in $NaCH_3CO_2 \cdot 3\,H_2O$: Comparison between a crystal and its glassy counterpart

A. J. Moreno, A. Alegría, and J. Colmenero
Departamento de Física de Materiales y Centro Mixto CSIC-UPV/EHU, Universidad del País Vasco (UPV/EHU), Apartado 1072, 20080 San Sebastián, Spain

B. Frick
Institute Laue-Langevin, BP 156X, F-38042 Grenoble, France
(Received 31 October 2001; published 19 March 2002)

Neutron-scattering measurements are carried out in order to study the temperature evolution of methyl-group dynamics in the same sample of sodium acetate trihydrate in crystalline and glassy state. The results in the crystalline sample are analyzed according to the usual single-particle assumption, and those in the glass in terms of a Gaussian distribution of single-particle potentials, this distribution resulting from the structural disorder present in the glass. It is found that the average potential barrier for the glass takes, within the experimental error, the same value as the single barrier in the crystal. The standard deviation of the distribution takes a value similar to those obtained in the quite different structural glasses (polymers) that were studied up to now. The reliability of some approximations introduced by the model for the dynamics of the individual methyl groups in the glass are tested in the crystalline phase.

DOI: 10.1103/PhysRevB.65.134202 PACS number(s): 61.43.Fs, 61.12.Ex, 61.41.+e

I. INTRODUCTION

Incoherent neutron scattering is a powerful tool for the study of single-particle motions of molecular groups containing hydrogen atoms, due to the large incoherent scattering cross section of the proton (80 barn, with 1 barn $=10^{-24}$ cm^2), in comparison with other nuclei. Moreover, a selective deuteration—the incoherent scattering cross section of deuterium is only 2 barn—allows one to enhance the contribution from the dynamics of a particular group of hydrogens in the spectra.

The dynamics of small rotors such as ammonia, methane, ammine ions, and particularly, methyl groups, has been investigated mainly by using this technique.[1–14] In most cases, the results of the relevant interactions on these rotors can be modeled as an effective single-particle rotational potential. The strong dependence of the rotational tunneling frequency on the potential barrier height allows one to determine the latter accurately by measuring the tunneling peaks, in combination with measurements of the torsional peaks and the activation energy for classical hopping.

Due to their quite simple dynamics, these rotors have been considered ideal systems for the development of theoretical models for a crossover from quantum tunneling to classical hopping.[15–19] Moreover, they have also given rise to a great experimental interest, and have often been used as internal dynamic probes to obtain information about their local environment[6–14] and the role of the different contributions to the effective rotational potential.[20–25] Some of the most representative cases of this kind of investigation are those concerning the effects of local disorder, which are reflected in distributions of rotational potential barriers. Though the idea of using such distributions for rotors in disordered environments is not new (see, e.g., Refs. 6, 10, and 20), a consistent model able to describe the spectra at every temperature (covering the tunneling, crossover, and hopping regimes), was lacking and only very recently was introduced. This model—the rotation—rate-distribution-model (RRDM) (Refs. 26–33)—is especially useful for an analysis of methyl-group dynamics in strongly disordered environments as in the case of structural glasses, which present broad distributions, reflected by the absence of well-defined tunneling peaks in neutron-scattering spectra[27,29–33] (see below). It is based on the idea that, in glasses, the spectra for methyl-group dynamics result from the superposition of unsolved crystallike spectra of the individual methyl groups. As exposed in Sec. II B, a few assumptions about the temperature dependence of the latter allow one to describe the spectra of the glass in terms of only three parameters.

A series of neutron-scattering studies[26–29,31] showed the suitability of the RRDM for glassy polymers; however, in principle, the grounds of the model are appliable to any disordered system. In contrast to glassy polymers, which cannot be obtained in a highly crystalline state, low molecular weight glasses allow a comparative study of the methyl-group dynamics in both states of the same sample. Such a comparison was recently made for toluene,[33] a system for which the interpretation is somewhat complex, due to the existence of two crystalline phases.[34] Toluene exists both in a stable ''α phase'' and a metastable ''β phase.'' The β phase shows a short-range order similar to the glassy phase,[35] and therefore it is the crystalline reference phase which has to be compared. However, the only information about the methyl-group rotational dynamics in β toluene is an early measurement of the tunneling peaks.[36] Due to the difficulty in retaining this metastable phase for a sufficiently long time, it was not possible to study such dynamics as a function of the temperature.[33]

Sodium acetate trihydrate is a more adequate system for this comparison. Methyl-group dynamics in the crystalline phase was investigated early by Clough and co-workers in a

wide temperature range.[37,38] The reported results suggest that this is a canonical system for methyl-group dynamics in the crystalline state, and that experimental results can be understood in terms of a single-particle potential.[37,38] For this reason, it is an ideal system to test the reliability of the different approximations introduced by the RRDM for the temperature dependence of the unsolved individual crystallike spectra. Moreover, it can be easily obtained in a glassy state with moderate cooling rates, and selective deuteration of the water molecules is possible in order to attenuate their contribution to the spectra.

In this work we present a neutron-scattering study of methyl-group dynamics in crystalline and glassy sodium acetate trihydrate. The different instruments used in the investigation cover a wide dynamical range from 0.5 μeV to 2 meV. In the case of a crystalline phase, our measurements complement those reported in Refs. 37 and 38, which were taken in a narrower energy window. The paper is organized as follows: In Sec. II we summarize the usual model for methyl group dynamics in crystalline systems and the grounds of the RRDM. In Sec. III we give experimental details. In Secs. IV and V we present and discuss the neutron scattering measurements in terms of the RRDM. Finally, conclusions are given in Sec. VI.

II. THEORETICAL ASPECTS

A. Crystalline systems

The usual model for methyl-group (MG) rotation in crystalline systems at $T \approx 1$ K is that of a rigid rotor tunneling through a one-dimensional potential (single-particle model), the Hamiltonian being

$$H = -\frac{\hbar^2}{2I}\frac{\partial^2}{\partial \Phi^2} + V(\Phi), \tag{1}$$

with I the moment of inertia of the methyl group around the threefold axis. The potential $V(\Phi)$ is restricted to take a rotational symmetry of the methyl group, and usually it is sufficient to retain only the first term of the Fourier expansion (threefold term): $V(\Phi) = V_3(1-\cos 3\Phi)/2$. Higher-order contributions are mostly small corrections to the main threefold term. The coupling of the wave functions of the three wells splits the torsional levels into the sublevels A and E, the latter consisting of the degenerate doublet (E_a, E_b). These labels correspond to irreducible representations of the symmetry group C_3. The frequency splitting between the sublevels A and E of the ground level is the tunneling frequency ω_t, which for weak and moderate barriers (V_3 below ≈ 700 K) can be detected by neutron scattering in the μeV range as two inelastic peaks of resolution width centered at $\pm \hbar \omega_t$. The incoherent scattering function for rotational tunneling in a threefold potential, normalized to scattering from one hydrogen, is[1,2]

$$S^{\mathrm{inc}}_{\mathrm{MG}}(Q,\omega) = \frac{5+4j_0(Qr)}{9}\delta(\omega) + \frac{2[1-j_0(Qr)]}{9} \times [\delta(\omega+\omega_t) + \delta(\omega-\omega_t)], \tag{2}$$

with $\hbar Q$ the momentum transfer and $\hbar \omega$ the energy transfer of the neutron. j_0 is the zeroth-order spherical Bessel function, and r the H-H distance in the methyl group ($r = 1.78$ Å).

When increasing the temperature, the coupling of the methyl group to the lattice phonons cannot be ignored, and the single-particle picture is no longer valid. At the same time, a ''crossover'' from the rotational tunneling regime to the classical hopping regime takes place. This fact is clearly reflected in the spectra (generally above ≈ 20 K for moderate barriers). The tunneling peaks broaden into Lorentzian lines and shift toward the central elastic line.[1–5] These inelastic Lorentzians involve $A \leftrightarrow E$ transitions.[16–18] At the same time, the same part of the elastic scattering involving transitions $E_a \leftrightarrow E_b$,[16–18] transforms into a Lorentzian quasielastic line around the elastic peak.[1–5] The temperature dependence of these inelastic and quasielastic broadenings is given by complicated expressions involving factors for the coupling of the rotor to the lattice modes, and sums of Bose factors over the phonon frequencies resonant in the librational energies.[16–18] Such expresions can be well approximated by an Arrhenius law[1–5] driven by the first librational energy E_{01}, i.e.,

$$\Gamma_{AE} = \gamma_{AE}\exp(-E_{\mathrm{br}}/kT), \tag{3}$$

$$\Gamma_{E_aE_b} = \gamma_{E_aE_b}\exp(-E_{\mathrm{br}}/kT), \tag{4}$$

with $E_{\mathrm{br}} \approx E_{01}$. Γ_{AE} and $\Gamma_{E_aE_b}$ are, respectively, the half-width at half-maximum (HWHM) of the inelastic and quasielastic Lorentzians. The shift of the tunneling peaks is determined in a similar way, though in this case the sum is done over the whole phonon spectrum,[16–18] resulting in a lower activation energy, E_S, though close to E_{01}:

$$\hbar \Delta\omega_t = \gamma_{\mathrm{sh}}\exp(-E_S/kT). \tag{5}$$

The quantities γ_{AE}, $\gamma_{E_aE_b}$ and γ_{sh} in Eqs. (3)–(5) are temperature-independent preexponential factors. The incoherent scattering function in the crossover regime is[3]

$$S^{\mathrm{inc}}_{\mathrm{MG}}(Q,\omega) = \frac{1+2j_0(Qr)}{3}\delta(\omega) + \frac{2[1-j_0(Qr)]}{9} \times \{L(\omega;\Gamma_{E_aE_b}) + L[\omega+(\omega_t-\Delta\omega_t);\Gamma_{AE}] + L[\omega-(\omega_t-\Delta\omega_t);\Gamma_{AE}]\}. \tag{6}$$

The onset of the classical hopping regime takes place around ~ 50 K for moderate barriers, and it is characterized in the spectra by a merging of the inelastic and quasielastic Lorentzians into a single quasielastic Lorentzian, which broadens according to an Arrhenius law[1,2,5]

$$\Gamma = \Gamma_\infty \exp(-E_A/kT), \tag{7}$$

with E_A the activation energy for classical hopping, defined as the difference between the top of the barrier and the ground state. Γ_∞ is a temperature-independent preexponential factor. The merging takes place in a narrow temperature interval ($\Delta T \approx 7$–10 K). In the following, we will neglect

the width of this interval, and we will represent it as a unique temperature T_c, that will be referred to as the ''crossover temperature,'' that marks the onset of the classical behavior. The incoherent scattering function for the classical hopping regime is[1]

$$S^{\rm inc}_{\rm MG}(Q,\omega)=\frac{1+2j_0(Qr)}{3}\,\delta(\omega)+\frac{2[1-j_0(Qr)]}{3}L(\omega;\Gamma). \tag{8}$$

It is straightforward to see that the crossover function [Eq. (6)] reduces to Eqs. (2) and (8) in the two temperature limits. At $T\approx 1$ K, $\Gamma_{AE},\Gamma_{E_aE_b}$, and $\Delta\omega_t\rightarrow 0$, recovering Eq. (2). At high temperatures, where the classical limit has been reached, the tunneling peaks are shifted to zero ($\Delta\omega_t=\omega_t$), recovering Eq. (8) if Γ_{AE} and $\Gamma_{E_aE_b}$ are now substituted for by the classical Γ.

B. Rotation-rate-distribution model

In a glass, the different local environments yield a different barrier V_3 for each methyl group and therefore, a barrier distribution $g(V_3)$. As a consequence, the spectrum of the glass results from a superposition of the crystallike spectra of the individual methyl groups, weighted by $g(V_3)$. Thus the corresponding incoherent scattering function for methyl group dynamics in a glass is obtained as

$$S^{\rm inc}_{\rm RRDM}(Q,\omega)=\int g(V_3)S^{\rm inc}_{\rm MG}(Q,\omega,V_3)dV_3, \tag{9}$$

where the individual functions $S^{\rm inc}_{\rm MG}(Q,\omega,V_3)$ are defined according to Eqs. (2), (6), and (8). Due the superposition of the individual spectra, the shift and broadening of the individual peaks, and their merging when reaching the classical regime, are not observable. For this reason, it is not evident which physical description (the crossover picture below T_c, or the classical one above T_c) must be taken for each methyl group at the respective temperature. This ambiguity can be removed by introducing a functional relationship between the crossover temperature for each methyl group and its barrier height, $T_c=T_c(V_3)$. The latter is obtained by taking into account that the classical behavior for a given methyl group will be reached when its rate for incoherent hopping becomes comparable to its rate for coherent tunneling. Thus we define T_c as the temperature where $\Gamma/\hbar\omega_t=1$ or, from Eq. (7),

$$kT_c=E_A/\ln(\Gamma_\infty/\hbar\omega_t). \tag{10}$$

As E_A and $\hbar\omega_t$ are obtained as direct functions of V_3 from the eigenvalues of H, T_c depends only on the barrier height V_3 and on the preexponential factor Γ_∞. This latter parameter is taken as barrier independent in a good approximation.[26,33]

As shown elsewhere,[31] we make the approximation $\gamma_{AE}=\gamma_{E_aE_b}$, and denote both factors as $\gamma_{\rm br}$. We further make the approximation $E_S=E_{01}$.[31] Experiments show typical ratios of $\Gamma_{E_aE_b}/\Gamma_{AE}\approx 0.5$ and $E_S/E_{01}\approx 0.7$. However, the simplifications introduced here seem reasonable in glassy systems, since such fine effects are hidden in the broad distributions of these parameters. We impose a ratio of 1 simply for ''aesthetic'' reasons.

Now we see that the parameters γ_{AE}, $\gamma_{E_aE_b}$, and $\gamma_{\rm sh}$ for each methyl group can also be expressed as functions of only V_3 and Γ_∞. Thus, as required by the continuity condition $\Gamma_{AE}(T_c)=\Gamma_{E_aE_b}(T_c)=\Gamma(T_c)$, we have

$$\gamma_{\rm br}=\Gamma_\infty\exp[(E_{01}-E_A)/kT_c]. \tag{11}$$

As, in the classical onset, the tunneling frequency will be shifted to zero, we have

$$\gamma_{\rm sh}=\hbar\omega_t\exp(E_{01}/kT_c). \tag{12}$$

By following the procedure shown, we only need to know Γ_∞ and the parameters of the distribution $g(V_3)$ to evaluate unambiguously all the quantities appearing in Eqs. (2)–(8), and therefore, the integral of Eq. (9) in the whole temperature range. Finally we add the incoherent contribution of the other atoms of the molecule and the coherent contribution, both assumed to be elastic,

$$S(Q,\omega)=e^{-2W(Q)}[\sigma_{\rm coh}S(Q)\,\delta(\omega)+(\sigma_{\rm inc}-\sigma^{\rm MG}_{\rm inc})\,\delta(\omega)+\sigma^{\rm MG}_{\rm inc}S^{\rm inc}_{\rm RRDM}(Q,\omega)], \tag{13}$$

with $\sigma_{\rm coh}$ and $\sigma_{\rm inc}$ the total coherent and incoherent cross-sections and $\sigma^{\rm MG}_{\rm inc}$ the incoherent cross-section of the three hydrogens of the methyl group. $\sigma_{\rm coh}S(Q)$ is the coherent static intensity. The Debye-Waller factor $e^{-2W(Q)}$ gives the intensity loss with increasing temperature due to vibrations. Function (13) is convoluted with the instrumental resolution for comparison with the experimental scattering function $S_e(Q,\omega)$.

III. EXPERIMENT

Two samples of sodium acetate trihydrate with protonated and deuterated water, [$NaCH_3COO\cdot 3H_2O$ (or ''$p9$'') and $NaCH_3COO\cdot 3D_2O$ (or ''$d6$'')] were used in the experiment. The corresponding scattering cross sections per molecule are $\sigma_{\rm coh}=49.8$ barn and $\sigma_{\rm inc}=724.1$ barn for the $p9$ sample, and $\sigma_{\rm coh}=72.7$ barn and $\sigma_{\rm inc}=254.7$ barn for the $d6$ one. For both samples $\sigma^{\rm MG}_{\rm inc}=240.8$ barn. The $d6$ sample was prepared from a $p9$ one, purchased from Aldrich Chemical Co. This latter was dried in a vacuum oven, and rehydrated with deuterated water. Previous differential scanning calorimetric measurements showed, for both samples, a glass transition temperature $T_g\approx 215$ K at a heating rate of 20 K/min. Neutron-scattering measurements were carried out by means of the spectrometers IN16 (backscattering), IN5, and IN6 (time-of-flight) at the Institute Laue-Langevin (ILL, Grenoble, France). Two flat samples of thickness 0.2 mm (protonated water) and 0.7 mm (deuterated water) filled in an aluminum container were used in the measurements. The corresponding transmisions were close to 90%, allowing one to neglect multiple-scattering effects in the Q range we were restricted to in our analysis (1.3–1.9 Å^{-1}). In order to obtain a glassy state, the samples in the crystalline state were

raised only a few degrees above their melting point (about 345 K) in order to avoid dehydration, and then were quickly cooled down. Once the measurements in the glassy samples were taken, they were recrystallized and measured again, recovering the crystalline spectra. The instrumental resolutions were calibrated at 10 K by a vanadium sample of thickness 1 mm, which shows purely elastic scattering. The raw data were corrected from the detector efficiency, sample container, and absorption by means of the ILL standard programms. The scattering angle (Φ), incident neutron beam energy (E_0), and momentum transfer Q and energy transfer $\hbar\omega$ of the scattered neutron are related through the equation (see, e.g., Ref. 39)

$$\hbar^2 Q^2/2m = 2E_0 + \hbar\omega - 2\sqrt{E_0(E_0+\hbar\omega)}\cos\Phi. \quad (14)$$

An incident wavelength of 6.27 Å was used in IN16, yielding a nearly Gaussian resolution with a HWHM of about 0.4 μeV. The measurements covered energy and angular windows from -15 to 15 μeV and from 11° to 149°, respectively. As the incident beam energy (2.1 meV) is much larger than the maximum energy transfer, Eq. (14) can be well approximated as

$$Q = (4\pi/\lambda_0)\sin(\Phi/2), \quad (15)$$

so the data for each angular value correspond to a unique Q. The corresponding Q range obtained in this way covered from 0.2 to 1.9 Å^{-1}. Wavelengths of 6.5 and 5.1 Å^{-1} were selected in IN5 and IN6 respectively, yielding Gaussian resolutions with HWHM's of about 25 μeV (for IN5) and 50 μeV (for IN6). The angular range extended from 16° to 123° (IN5) and from 15° to 115° (IN6). Each angle covered an energy window from -0.6 to 19.5 meV (IN5) and from -2 to 1600 meV (IN6). In these instruments the approximation of Eq. (15) is not valid, and the scattering function $S(Q,\omega)$ was obtained from $S(\Phi,\omega)$ by means of a standard interpolation program. We restricted the analysis to the quasielastic energy range -1 to 2 meV (IN5) and from -2 to 2 meV (IN6). The Q range obtained after this procedure extended from 0.7 to 1.7 Å^{-1} (IN5) and from 0.4 to 2.0 Å^{-1} (IN6).

IV. RESULTS

Figure 1 shows the IN16 and IN6 neutron-scattering spectrum for the crystalline $p9$ sample at some of the measured temperatures, showing the usual behavior described in Sec. II A: with increasing temperature the tunneling peaks broaden and shift to lower frequencies. At the same time, a quasielastic component appears around the elastic peak. Finally, the inelastic and quasielastic components merge into a quasielastic line, characteristic of the classical hopping regime.

Figures 2 and 3 show the IN16 and IN5 spectra for the glassy $d6$ sample, respectively. The tunneling peaks of the crystalline $d6$ sample are also shown in the spectrum at 2 K

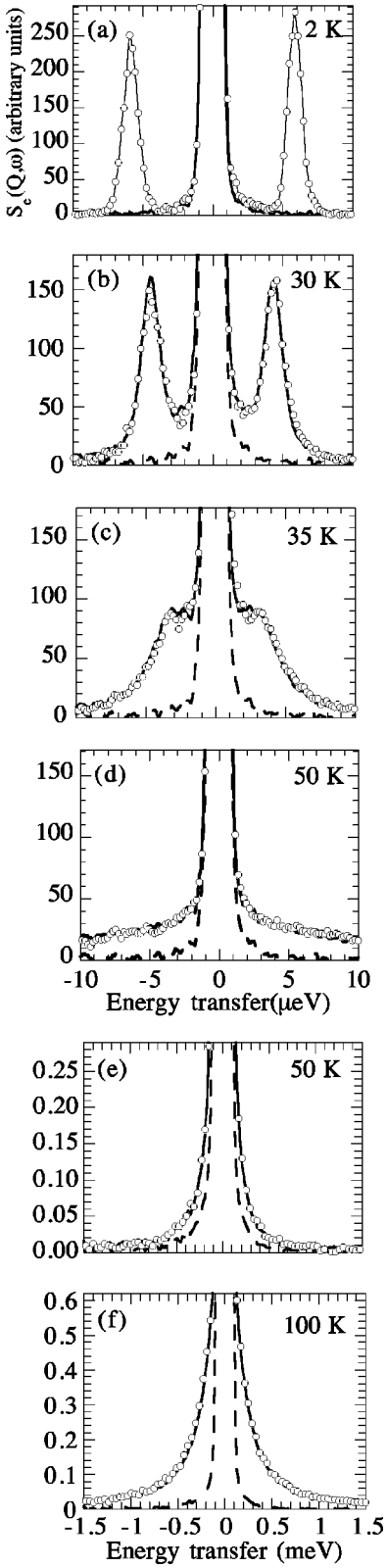

FIG. 1. Experimental spectra (points) for methyl-group dynamics in crystalline $p9$-sodium acetate trihydrate. Plots (a)–(d) correspond to IN16 and plots (e) and (f) to IN6. Solid lines are fits to the model for crystals exposed in Sec. II A. Dashed lines correspond to the experimental resolution. Scales refer to the maximum: (a) 8%, (b)–(d) 5%, (e) 1%, and (f) 3%.

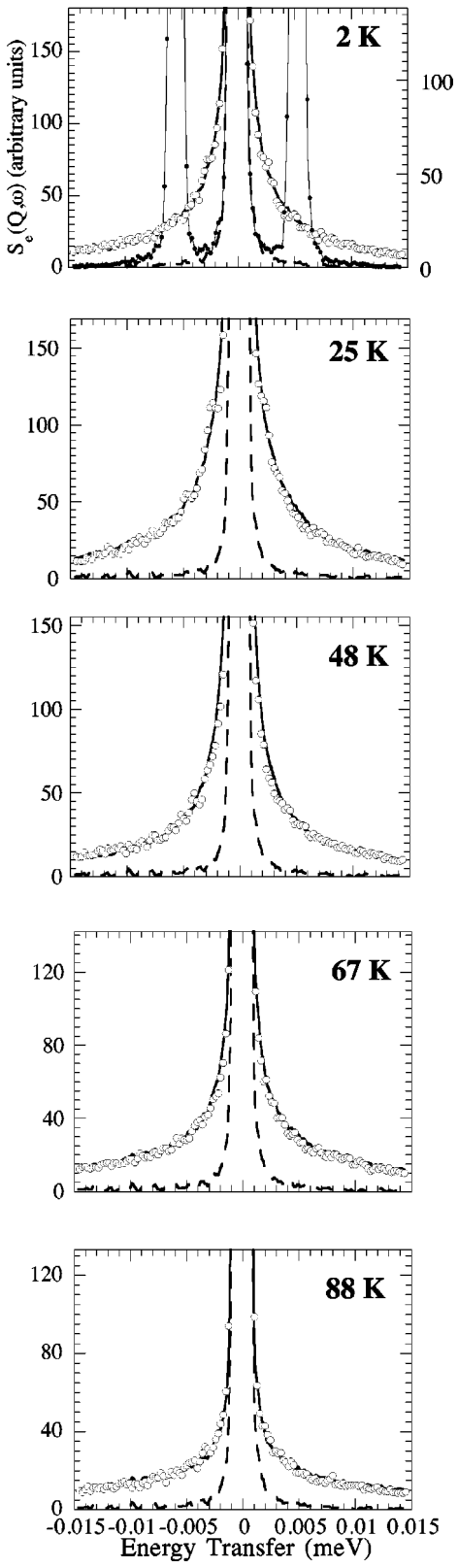

FIG. 2. Experimental IN16 spectra (open points) and theoretical curves given by the RRDM (solid thick lines) for glassy $d6$-sodium acetate trihydrate. The full points in the spectrum at 2 K correspond to the crystalline sample. The solid thin line is a guide for the eye. The dashed line in all the plots is the resolution function. The scale is 5% of the maximum.

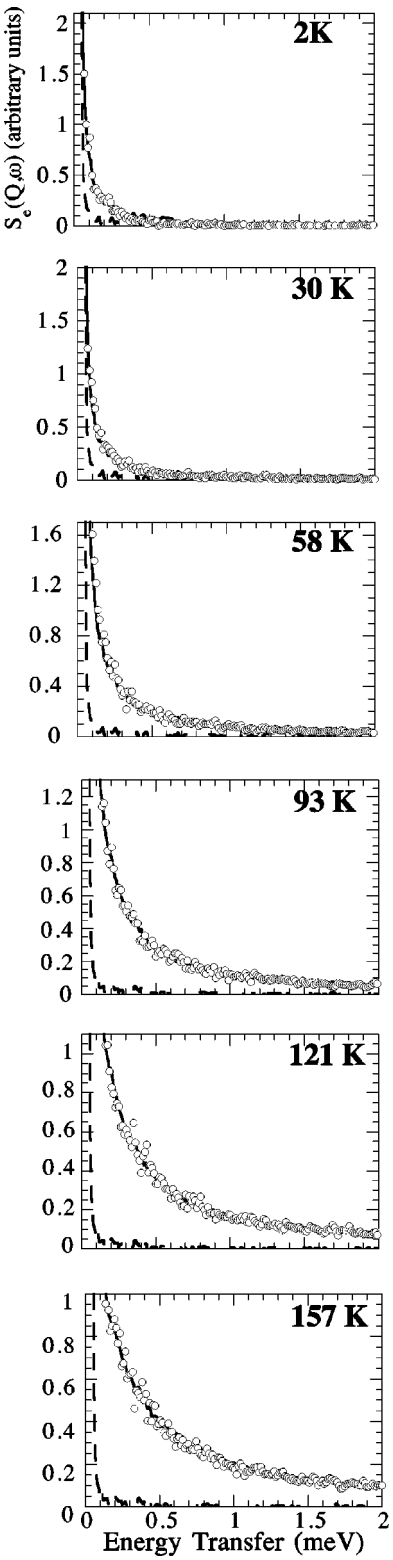

FIG. 3. As Fig. 2 for IN5 data. Scale: 2% of the maximum.

for comparison. As in the other structural glasses studied so far, the spectra do not show defined tunneling peaks, even at very low temperature, but a broad feature. In Sec. V we will show how such a feature can be described in terms of a superposition of crystallike spectra according to the model exposed in Sec. II B.

V. DISCUSSION

The tunneling frequency measured for the crystalline $p9$ sample, $\hbar\omega_t = 5.8$ μeV, is in agreement with the value published in Ref. 38. In the crystalline $d6$ sample, it is shifted to $\hbar\omega_t = 5.4$ μeV (see Fig. 2). In a pure threefold assumption the corresponding barrier height is increased slightly from $V_3 = 403$ K to $V_3 = 411$ K. Similar effects due to slight changes of the interatomic distances of the lattice upon deuteration were also reported in other systems.[40]

The spectra in Fig. 1 were fitted (solid lines) to the usual model for crystalline systems exposed in Sec. II A, -i.e., by taking Eqs. (2), (6), and (8) for $S^{\rm inc}_{\rm MG}(Q,\omega)$ in the different regimes. The total coherent contribution as well as the incoherent contribution of the other atoms were added as in Eq. (13), and the theoretical function constructed this way was convoluted with the instrumental resolution. The Debye-Waller factor only affects the scattering function as a scaling factor for each Q value, and was not taken into account in the analysis procedure, where the theoretical function was scaled to the experimental maximum at each Q value. Information about the coherent static intensity is not available. We approximated $S(Q)$ to unity due to the small contribution of the latter to the total elastic peak (below 9% for this approximation). In the analyzed Q-range we did not observe significantly higher elastic intensities that could be asigned to Bragg peaks and would contradict such an approximation.

The quantities $\Delta\omega_t$, Γ_{AE}, $\Gamma_{E_aE_b}$, and Γ in Eqs. (2), (6), and (8) were taken as fitting parameters. Figure 4 shows the temperature dependence of these latter parameters. No broadenings could be resolved at temparatures below 24 K. The curves for Γ_{AE}, $\Gamma_{E_aE_b}$, and Γ follow the general behavior observed in crystals: they intersect in a somewhat ill-defined ''crossover temperature'' [from Fig. 4(e), $T_c \sim 45$ K], with a strong change in the activation energy when crossing T_c. Contrary to what is usually observed, Γ_{AE} takes lower values than $\Gamma_{E_aE_b}$, although of the same order of magnitude.

Data of Ref. 38 are also represented for comparison. The agreement between both measurements is good for $\Delta\omega_t$ and Γ_{AE}. Conversely, the values of $\Gamma_{E_aE_b}$ are clearly uncompatible with a common Arrhenius law. The strong discrepancy with our results might be due to the insufficiently good quality of the former measurements and the quite indirect method used to separate the quasielastic line from the elastic peak.[38]

The dashed lines in Fig. 4 correspond to fits of our data to Arrhenius laws like $\gamma\exp(-E/kT)$. Table I shows the values of γ and E obtained from such fits. In a pure threefold approximation, the first librational energy and the classical activation energy for the potential $V_3 = 403$ K of the crystalline $p9$ sample are $E_{01} = 12.6$ meV (146 K) and $E_A = 327$ K, respectively. The activation energies given in Table I are close to E_{01} for $\hbar\Delta\omega_t$, Γ_{AE}, and $\Gamma_{E_aE_b}$, and to E_A for Γ. Thus, one has the relationships $E/E_{01} = 0.86$, 1.3, and 0.86 and $E/E_A = 0.89$, respectively. The preexponential factors γ take values similar to those typically observed in other systems. Thereby, sodium acetate trihydrate is con-

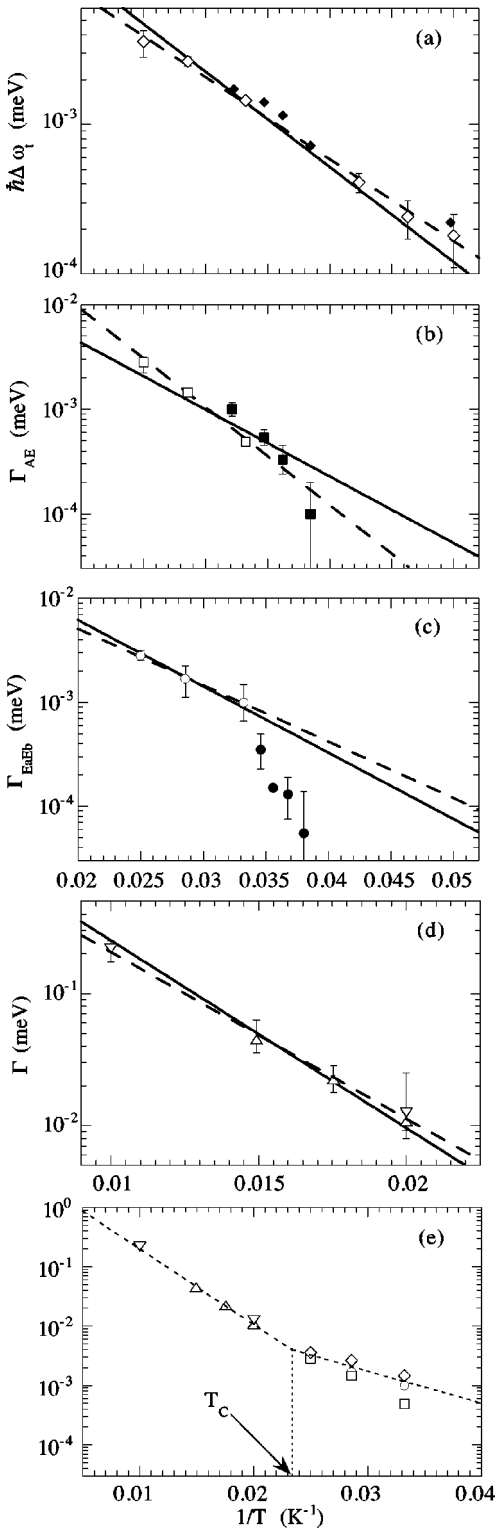

FIG. 4. Temperature dependence of the shift of the tunneling frequency and of the crossover and classical Lorentzian broadenings for the crystalline $p9$ sample. Open points correspond to our IN16 data, except for the inverted triangles in (d) and (e), which correspond to our IN6 data. The data reported in Ref. 38 are also plotted for comparison (full points). See the text for the meaning of the solid and dashed lines in (a)–(d). Plot (e) shows all the above data in the same frame. The arrow marks the crossover temperature. Dotted lines are a guide for the eyes.

TABLE I. Preexponential factors and activation energies for the shifts and line broadenings for crystalline $NaCOOCH_3 \cdot 3H_2O$.

	$\hbar\Delta\omega_t$	Γ_{AE}	$\Gamma_{E_aE_b}$	Γ
γ (meV)	0.090	0.34	0.063	3.8
E (K)	126	196	125	292

firmed as a canonical system for methyl-group dynamics in crystalline systems.

The values of $\hbar\Delta\omega_t$, Γ_{AE}, $\Gamma_{E_aE_b}$, and Γ were again fitted to Arrhenius laws, but fixing the activation energies to the values of E_{01} (of E_A in the case of Γ) corresponding to $V_3 = 403$ K, and leaving the preexponential factors γ as fitting parameters. The solid lines in Fig. 4 show such fits. The values of the preexponential factors obtained from this procedure are given in Table II. These values can be compared with those predicted by Eqs. (10)–(12), resulting from the approximations introduced by the RRDM for the temperature dependence of the individual spectra. Thus the crossover temperature defined as Eq. (10) takes a value $T_c = 47$ K, in agreement with the experimental observation. By introducing this latter value in Eqs. (11) and (12), we have $\gamma_{\mathrm{br}} = \gamma_{\mathrm{sh}} = 0.135$ meV, close to the values given in Table II. These results illustrate the reliability of the introduced approximations.

Concerning the glassy $d6$ sample, we followed the usual procedure to analyze the data in terms of the convolution of Eq. (13) with the instrumental resolutions.[26–33] As in the crystalline sample, $S(Q)$ could be well approximated to unity. Taking into account that low-energy vibrations are expected to contribute in the IN5 window, a flat background was introduced as an additional parameter in the analysis of the IN5 data. A Gaussian form for the distribution $g(V_3)$ was assumed,

$$g(V_3) = (1/\sqrt{2\pi}\sigma_V)\exp[-(V_3 - V_{3_0})^2/2\sigma_V^2], \qquad (16)$$

with V_{3_0} the average barrier and σ_V the standard deviation. Due to the independence of the preexponential factor Γ_∞ on the barrier height, Eq. (7) establishes a linear dependence of $\log\Gamma$ on E_A. As E_A depends linearly on V_3 in a good approximation,[29,32] the distribution of classical activation energies $f(E_A)$ and classical Lorentzian broadenings $H(\log\Gamma)$ take the same functional form as $g(V_3)$, and are Gaussian in the present case. With all these considerations in mind, experimental spectra were first fitted to the classical limit of the model, i.e., by taking the classical form of Eq. (9),

TABLE II. Preexponential factors (in meV) for the shifts and line broadenings for crystalline $NaCOOCH_3 \cdot 3H_2O$, with the activation energies fixed to E_{01} (to E_A in the case of Γ).

γ_{sh}	γ_{AE}	$\gamma_{E_aE_b}$	Γ_∞
0.19	0.082	0.12	6.6

$$S^{\mathrm{inc}}_{\mathrm{RRDM}}(Q,\omega) = \int H(\log\Gamma) S^{\mathrm{inc}}_{\mathrm{MG}}(Q,\omega,V_3)\, d\log\Gamma, \quad (17)$$

with $S^{\mathrm{inc}}_{\mathrm{MG}}(Q,\omega,V_3)$ given by Eq. (8). This procedure enables calculations of the preexponential factor Γ_∞, the average activation energy E_{A_0}, and the standard deviation σ_E of $f(E_A)$ from fitting the series of average values $\log\Gamma_0$ and standard deviations σ of $H(\log\Gamma)$ obtained at each temperature to the equations[26,28,32,33]

$$\log\Gamma_0 = \log\Gamma_\infty - [E_{A_0}\log(e)/kT], \qquad (18)$$

$$\sigma = \sigma_E \log(e)/kT. \qquad (19)$$

As shown in Figs. 5 and 6, the values of $\log\Gamma_0$ and σ below ≈ 60 K deviate from the linear behavior given by Eqs. (18) and (19), indicating the breakdown of the classical model and the contribution of quantum effects below this temperature. For this reason, only the set of values $(\log\Gamma_0, \sigma)$ obtained above 60 K was fitted to the latter equations, yielding the parameters $\Gamma_\infty = 4.9$ meV, $E_{A_0} = 335$ K, and $\sigma_E = 182$ K.

The eigenvalues of Hamiltonian (1) were calculated by a standard diagonalization procedure for different values of V_3. The set of values $(V_3, E_A, E_{01}, \hbar\omega_t)$ obtained in this way allowed a transformation of the distribution $f(E_A)$ obtained in the high-temperature analysis into the barrier distribution $g(V_3)$. The obtained parameters of $g(V_3)$ are 417 K for the average barrier and 194 K for the standard deviation. The two latter parameters yield an unphysical result: $g(V_3)$ presents a significant population of negative values of V_3 (below $V_{3_0} - 2.15\sigma_V$). For this reason, another analysis was made, imposing a cutoff at zero energy, and normalizing the distributions to the unit area. The fit yielded, within the error bar, the same parameters as found above. It is worthy of remark that, in this case, the parameters V_{3_0} and σ_V that characterize $g(V_3)$ do not correspond to the average barrier and the standard deviation, since the distribution has been truncated at zero energy. The actual average barrier $V^c_{3_0}$ and standard deviation σ^c_V of the truncated distribution $g^c(V_3)$ were calculated as

$$V^c_{3_0} = \langle V_3\rangle = \frac{\int V_3 g^c(V_3) dV_3}{\int g^c(V_3) dV_3}, \qquad (20)$$

$$\sigma^c_V = \sqrt{\langle V_3^2\rangle - \langle V_3\rangle^2}, \qquad (21)$$

yielding the values $V^c_{3_0} = 425$ K and $\sigma^c_V = 185$ K.

Once the RRDM parameters were determined, the theoretical scattering function [Eq. (13)] was calculated by taking the general expression [Eq. (9)] of $S^{\mathrm{inc}}_{\mathrm{RRDM}}(Q,\omega)$ instead of its classical limit [Eq. (17)]. It must be noted that this latter calculation does not involve any fitting procedure, i.e., the spectra are *simulated* with the distribution $g(V_3)$ and the preexponential factor Γ_∞ calculated in the high-temperature fitting procedure, and *compared* with the experimental data. Figures 2 and 3 show the excellent agreement between theory and experiment in the whole temperature range.

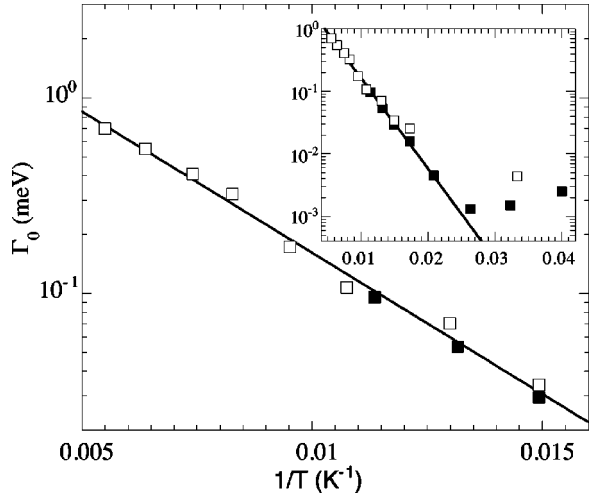

FIG. 5. Temperature dependence for the broadening of the Lorentzian for classical hopping corresponding to the average barrier in the glassy $d6$ sample. The line is a fit to Eq. (18). Black points: IN16; white points: IN5. The inset depicts the points in the whole temperature range.

Figure 7 shows the distribution of crossover temperatures $G(T_c)$ that follows from $g(V_3)$ through Eq. (10). As can be seen in the figure, the population of barriers with T_c above ≈ 60 K is nearly negligible, and therefore it is below this temperature where the classical hopping limit of the RRDM breaks, as already indicated in Figs. 5 and 6, and where the general model must be taken.

In order to follow the temperature evolution of the spectra in more detail, we depict integrated intensities (points) in different inelastic windows in Fig. 8, together with the theoretical curves (solid lines) calculated in the framework of the RRDM with the above parameters. The latters have been modulated by a Debye-Waller factor $\exp(-2Q^2\langle u^2\rangle/3)$, to give account for the intensity decay due to vibrations. A

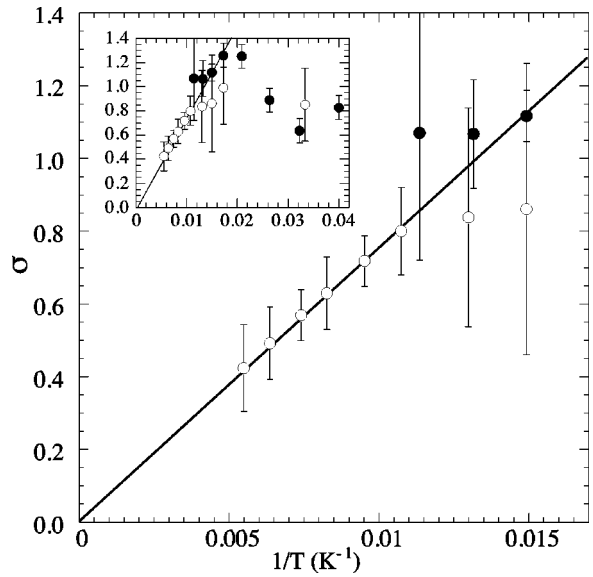

FIG. 6. As Fig. 5 for the standard deviation of the distribution $H(\log\Gamma)$. The line is a fit to Eq. (19).

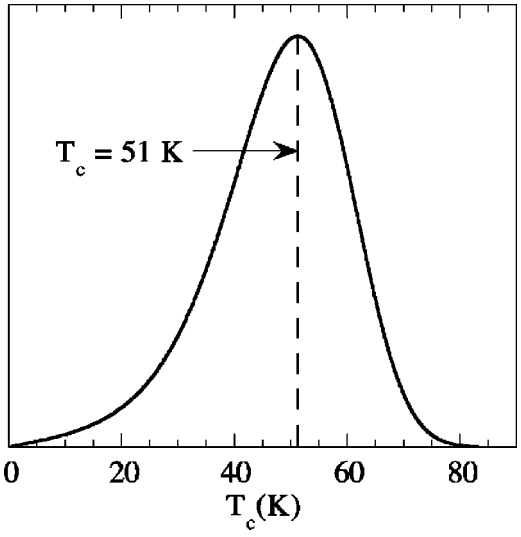

FIG. 7. Distribution of crossover temperatures for the glassy $d6$ sample.

mean-squared displacement $\langle u^2\rangle = 3\times 10^{-4}T$ has been assumed.[41] The agreement between experiment and theory is again excellent. The description in terms of the hopping limit has been extrapolated to low temperature (dashed lines). It is clear that the intensity excess below ≈ 60 K, due to the methyl groups not having reached the hopping regime, is reproduced by the general RRDM.

Finally we make a comment about preliminary study of the tunneling spectrum of glassy $p9$-sodium acetate trihydrate with protonated water (see Ref. 30). There we reported a value of $\sigma_V = 218$ K, similar to that calculated in this study, but a quite different value of $V_{3_0} = 592$ K. Moreover, the application of the RRDM with these parameters could not give account for the experimental data at higher temperatures. Such parameters were wrongly calculated, since the

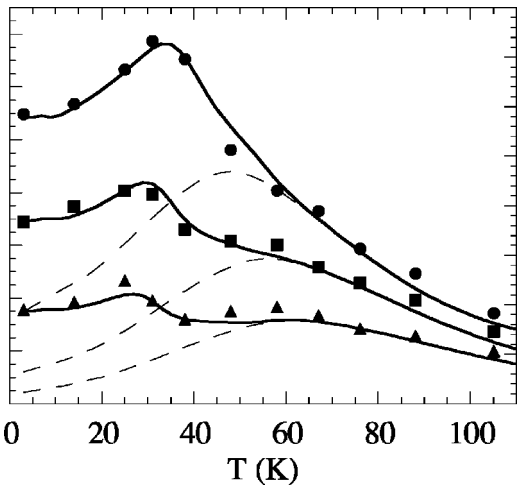

FIG. 8. Integrated intensities for the glassy $d6$ sample at $Q = 1.75$ Å^{-1} in the ranges 1–3 μeV (circles), 3–6.5 μeV (squares), and 6.5–10 μeV (triangles). Solid lines are the values predicted by the RRDM. Dashed lines correspond to a description exclusively in terms of classical hopping.

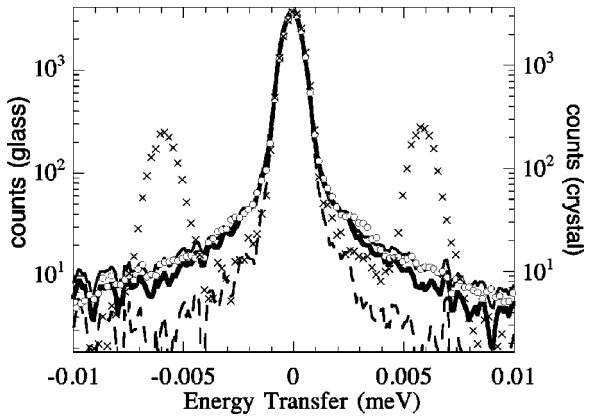

FIG. 9. Logarithmic plot of the IN16 spectrum at 2 K for the $p9$ sample in crystalline (crosses) and glassy state (circles). The solid lines are the theoretical RRDM functions for the parameters given in this work (thin) and in Ref. 30 (thick). The dashed line is the instrumental resolution.

theoretical scattering function was convoluted with an insufficiently well-modeled resolution, instead of with the actual experimental resolution. Due to the high contribution of the elastic peak in the $p9$ sample (for $Q=1.8$ Å^{-1}, 76% of the total intensity, while only 43% for the $d6$ sample), the convolution with such a model resolution led to the wrong parameters. Here a calculation was made in the $p9$ sample by using the actual experimental resolution. Figure 9 shows the spectrum of such a sample at 2 K in the glassy state with the theoretical curves corresponding to the wrong parameters of Ref. 30, and the actual ones presented in this study. It is now clear that it is the latter which reproduce correctly the spectrum. Moreover, they also give account of the experimental data in the whole temperature range, as shown in the intensity diagram of Fig. 10 and in the IN6 spectra of Fig. 11. In this way, it is proved that the parameters of the RRDM reported in this study achieve a consistent description of the experimental spectra in both samples and at every temperature.

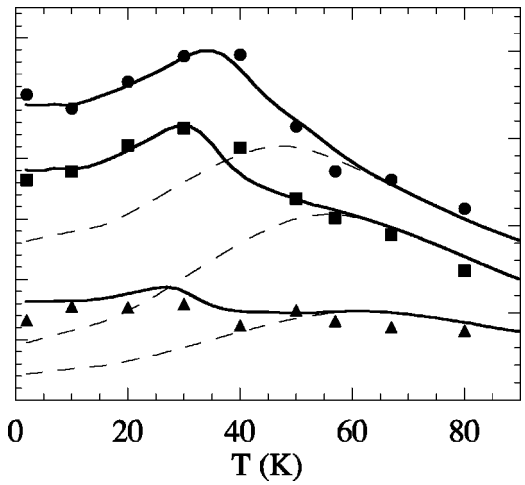

FIG. 10. As Fig. 8, for the glassy $p9$ sample. The ranges are 1–2.5 μeV (circles), 2.5–6.5 μeV (squares), and 6.5–10 μeV (triangles).

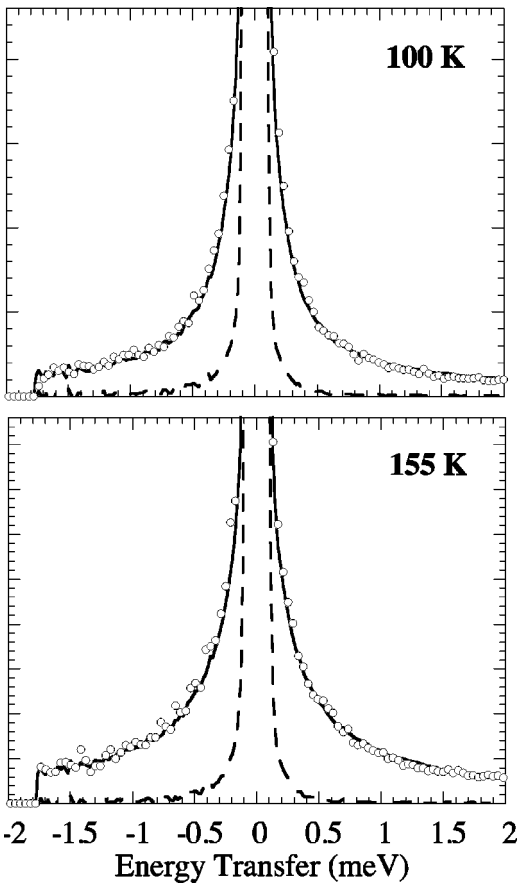

FIG. 11. As Fig. 2, for the IN6 data in the glassy $p9$ sample. Scale: 2% of the maximum.

VI. CONCLUSIONS

Neutron-scattering measurements have been carried out to determine the parameters of the distribution of potential barriers for methyl-group rotation in glassy sodium acetate trihydrate. A consistent description in terms of the RRDM has been achieved. The obtained distribution has an average barrier of 425 K, equal, within the experimental error, to the single barrier in the crystal, so that the only effect of the disorder is to distribute the values of the barrier around the latter. The value for standard deviation of the distribution, 185 K, is similar to those obtained in polymers[26–29,31,32] and other quite different structural glasses. The approximations introduced by the RRDM for the temperature dependence of the individual unresolved crystallike spectra that contribute to the total spectrum of the glass have been tested in the crystalline phase. Such approximations have been proved to be consistent with the results obtained in the latter.

ACKNOWLEDGMENTS

This work was supported by Project Nos. DGICYT, PB97-0638; GV, EX 1998-23; UPV/EHU, and 206.215-G20/98. The support from DIPC and Iberdrola S.A. are also acknowledged. We thank L. Leza for sample preparation, I. Tellería for DSC measurements, and H. Casalta for experimental help.

[1] W. Press, *Single-Particle Rotations in Molecular Crystals*, Springer Tracts in Modern Physics, Vol. 92 (Springer, Berlin, 1981).
[2] M. Prager and A. Heidemann, Chem. Rev. **97**, 2933 (1997).
[3] M. Prager, K. H. Dupŕee, and W. Müller-Warmuth, Z. Phys. B: Condens. Matter **51**, 309 (1983).
[4] D. Cavagnat, A. Magerl, C. Vettier, and S. Clough, J. Phys. C **19**, 6665 (1986).
[5] A. Heidemann, M. Prager, and M. Monkenbusch, Z. Phys. B: Condens. Matter **76**, 77 (1989).
[6] S. Grondey, M. Prager, W. Press, and A. Heidemann, J. Chem. Phys. **85**, 2204 (1986).
[7] M. Prager and W. Langel, J. Chem. Phys. **88**, 7995 (1988).
[8] F. Leclerq, P. Damay, and P. Chieux, J. Phys. Chem. **94**, 7300 (1990).
[9] B. Asmussen, M. Prager, W. Press, H. Blank, and C. J. Carlile, J. Chem. Phys. **97**, 1332 (1992).
[10] B. Asmussen, W. Press, M. Prager, and H. Blank, J. Chem. Phys. **98**, 158 (1993).
[11] M. Prager, B. Asmussen, W. Langel, C. J. Carlile, and H. Blank, J. Chem. Phys. **99**, 2052 (1993).
[12] M. Prager, B. Asmussen, and C. J. Carlile, J. Chem. Phys. **100**, 247 (1994).
[13] C. Gutt, B. Asmussen, I. Krasnov, W. Press, W. Langel, and R. Kahn, Phys. Rev. B **59**, 8607 (1999).
[14] R. M. Dimeo and D. A. Neumann, Phys. Rev. B **63**, 014301 (2001).
[15] S. Clough, A. Heidemann, A. J. Horsewill, J. D. Lewis, and M. N. J. Paley, J. Phys. C **15**, 2495 (1982).
[16] A. C. Hewson, J. Phys. C **15**, 3841 (1982).
[17] A. Würger, Z. Phys. B: Condens. Matter **76**, 65 (1989).
[18] A. Hüller, Z. Phys. B: Condens. Matter **78**, 125 (1990).
[19] S. Clough, A. J. Horsewill, and M. R. Johnson, Phys. Rev. A **47**, 3420 (1993).
[20] C. Bostoen, G. Coddens, and W. Wegener, J. Chem. Phys. **91**, 6337 (1989).
[21] M. R. Johnson, B. Frick, and H. P. Trommsdorff, Chem. Phys. Lett. **258**, 187 (1996).
[22] M. R. Johnson, M. A. Neumann, B. Nicolai, P. Smith, and G. J. Kearley, Chem. Phys. **215**, 343 (1997).
[23] M. R. Johnson, M. Prager, H. Grimm, M. A. Neumann, G. J. Kearley, and C. C. Wilson, Chem. Phys. **244**, 49 (1999).
[24] M. A. Neumann, M. R. Johnson, P. G. Radaelli, H. P. Trommsdorff, and S. F. Parker, J. Chem. Phys. **110**, 516 (1999).
[25] F. Alvarez, A. Alegría, J. Colmenero, T. M. Nicholson, and G. R. Davies, Macromolecules **33**, 8077 (2000).
[26] A. Chahid, A. Alegría, and J. Colmenero, Macromolecules **27**, 3282 (1994).
[27] J. Colmenero, R. Mukhopadhyay, A. Alegría, and B. Frick, Phys. Rev. Lett. **80**, 2350 (1998).
[28] R. Mukhopadhyay, A. Alegría, J. Colmenero, and B. Frick, Macromolecules **31**, 3985 (1998).
[29] A. J. Moreno, A. Alegría, J. Colmenero, and B. Frick, Phys. Rev. B **59**, 5983 (1999).
[30] A. J. Moreno, A. Alegría, J. Colmenero, and B. Frick, Physica B **276-278**, 361 (2000).
[31] A. J. Moreno, A. Alegría, and J. Colmenero, Phys. Rev. B **63**, 060201(R) (2001).
[32] A. J. Moreno, A. Alegría, J. Colmenero, and B. Frick, Macromolecules **34**, 4886 (2001).
[33] A. J. Moreno, A. Alegría, J. Colmenero, M. Prager, H. Grimm, and B. Frick, J. Chem. Phys. **115**, 8958 (2001).
[34] J. Bruneaux-Poulle, L. Bossio, and M. Dupont, J. Chim. Phys. Phys.-Chim. Biol. **76**, 333 (1979).
[35] J. Bruneaux-Poulle, A. Defrain, and M. Dupont, J. Chim. Phys. Phys.-Chim. Biol. **78**, 217 (1981).
[36] D. Cavagnat and W. Petry, ILL Exp. Report No. 09-03-566, 1989 (unpublished).
[37] S. Clough, A. Heidemann, M. N. J. Paley, and J. B. Suck, J. Phys. C **13**, 6599 (1980).
[38] S. Clough, A. Heidemann, and M. N. J. Paley, J. Phys. C **14**, 1001 (1981).
[39] M. Bée, *Quasielastic Neutron Scattering: Principles and Applications in Solid State Chemistry, Biology and Materials Science* (Hilger, Bristol, 1988).
[40] D. Cavagnat, S. F. Trevino, and A. Magerl, J. Phys.: Condens. Matter **1**, 10047 (1989).
[41] B. Frick and L. J. Fetters, Macromolecules **27**, 974 (1994).